JOURNAL OF MAGNETIC RESONANCE **131,** 1–7 (1998)
ARTICLE NO. MN971336

Quadrupole–Dipole Effects in Solid-State, CP-MAS, Tin-119 NMR Spectra of *para*-Substituted Triaryltin(pentacarbonyl)manganese(I) Complexes

Dharamdat Christendat, Ivor Wharf, Frederick G. Morin, Ian S. Butler,[1] and Denis F. R. Gilson[1]

Department of Chemistry, McGill University, 801 Sherbrooke St. West, Montreal, Quebec, Canada H3A 2K6

Received April 1, 1997; revised November 25, 1997

Solid-state, CP-MAS, ^{119}Sn NMR spectra were measured for a series of *para*-substituted triaryltin(pentacarbonyl)manganese(I) complexes. All the spectra show an asymmetric sextet due to spin–spin coupling and second-order quadrupolar effects, transmitted by dipolar coupling between the ^{119}Sn and ^{55}Mn nuclei, which are not suppressed by magic-angle rotation. The solid-state $^1J_{Mn-Sn}$ spin–spin and nuclear quadrupole coupling constants range from 130 to 250 Hz and −8 to 21 MHz, respectively, and show an inverse linear correlation, which is attributed to the dominance of the Fermi contact contribution to the $^1J_{Mn-Sn}$ coupling. The tris(*p*-methylthiophenyl)tin derivative is an exception, attributed to a difference in crystal structure from the other complexes. The magnitudes of the principal elements of the ^{119}Sn chemical shift tensors were determined and appear to be strongly influenced by the ring torsion angles and the *para*-substituents of the phenyl rings. Solid-state ^{119}Sn NMR spectroscopy provides a useful method of probing the electronic environment around the tin and manganese nuclei in transition metal complexes.

INTRODUCTION

Solid-state, CP-MAS, ^{119}Sn NMR spectra of organometallic complexes containing a quadrupolar nucleus have proved particularly useful in recent years in understanding the structures, bonding interactions, and molecular dynamics of organotin complexes (*1–5*). However, there has not yet been a solid-state NMR study reported concerning covalent bimetallic (i.e., directly bonded metal atoms) complexes involving tin (or any other Group 14 (IVA) element) and a transition metal. Examples of such bimetallic compounds containing manganese carbonyl and triorganotin fragments were first prepared many years ago by Gorsich (*6*) and Jetz *et al.* (*7*), and the triorganotin radicals in the $R_3SnMn(CO)_5$ compounds were characterized as good σ-donors and π-acceptors on the basis of infrared, Raman, and X-ray crystallographic data (*7–11*). Most of the theoretical and experimental work on *para*-substituted tri- and tetra-aryltin complexes has involved solution studies of the isotropic tin-119 chemical shifts and spin–spin coupling ($^nJ_{C-Sn}$) between ^{13}C and ^{119}Sn, and it has been found that small changes in molecular structure can lead to significant changes in both of these parameters (*12, 13*). These changes have been related to the electronegativities of the substituents, their σ- and π-bonding character, and the coordination state of the tin atom (*12*).

The objective of the present study was to investigate the effects of *para*-substituents on the aryl rings in the solid-state, CP-MAS, ^{119}Sn NMR spectra of a series of (*para*-$XC_6H_4)_3Sn(CO)_5Mn$ [X = H, F, Cl, CH_3, OCH_3, SCH_3, and $S(O)_2CH_3$] derivatives. The specific parameters under investigation were the manganese–tin spin–spin coupling constants ($^1J_{Mn-Sn}$), the effective dipolar coupling constants, and the ^{55}Mn quadrupole coupling constants. This study provides an opportunity to examine the relationship between the $^1J_{Mn-Sn}$ coupling and the nuclear quadrupole coupling constant, χ, in these triaryltin(pentacarbonyl)manganese(I) derivatives.

If the Fermi contact term is the dominant mechanism of spin–spin coupling, then the $^1J_{X-Y}$ coupling values will increase as the *s*-bonding character increases (*14*),

$$J_{XY} \propto \gamma_X\gamma_Y|n_XS(0)|^2|n_YS(0)|^2\alpha_X^2\alpha_Y^2(\Delta E)^{-1}, \quad [1]$$

where γ is the nuclear magnetogyric ratio, $|nS(0)|^2$ is the electron density at the nucleus, α^2 is the *s*-character of the hybrid used in the bonding orbital, and ΔE represents the average excitation energy approximation. The opposite effect is predicted for the NQR coupling constant because, according to the theory of Dailey and Townes, as the *s*-bonding character increases the field gradient at the nucleus decreases (*15*),

$$q_{zz} = (1 - s - I - \pi)q_{at}, \quad [2]$$

where q_{zz} is the largest component of the electric field gradient, q_{at} is the atomic field gradient, and s, I, and π are the s, ionic, and double bond characters, respectively.

[1] To whom correspondence should be addressed.

1090-7807/98 $25.00

It was shown earlier by Gilson that a relationship exists between the one-bond carbon hydrogen spin–spin coupling constants, $^1J_{C-H}$, and halogen nuclear quadrupole coupling constants in mono-, di-, and trihalogenated methanes (*16*).

EXPERIMENTAL

The *para*-substituted triaryltin(pentacarbonyl)manganese(I) complexes were prepared and characterized as described previously (*13*).

The solid-state ^{119}Sn NMR spectra were recorded at 111.723 and 37.252 MHz using Chemagnetics M-300 (7.05 T) and M-100 (2.35 T) spectrometers, respectively, under conditions of ^{1}H–^{119}Sn cross-polarization, high-power proton decoupling and magic-angle spinning. Chemical shifts are given with respect to external tetramethyltin, $(CH_3)_4Sn$, using the chemical shift of solid tetracyclohexyltin, −97.0 ppm, as an external secondary reference (*17*). The CP-MAS spectra were obtained for approximately 250–300 mg of sample packed into zirconia pencil-type rotors (7.5-mm diameter), using a recycle time of 2–10 s, depending on the proton T_1 value, and a contact time of 1–3 ms. The number of transients ranged from 5000 to 35,000, depending on the complex in question. Line broadening of 0 and 10 Hz was applied and the FIDs were zero filled to 8K and 4K points on the M-300 and M-100 instruments, respectively, before transformation. Different spinning rates, ranging from 1.0 to 4.5 kHz, were used to identify the isotropic peaks. Band fits were performed on the center and spinning sidebands by using the program Peakfit (Jandel Scientific). Calculation of the shielding tensors was performed with the aid of a computational package developed by Kentgens *et al.* (*18*).

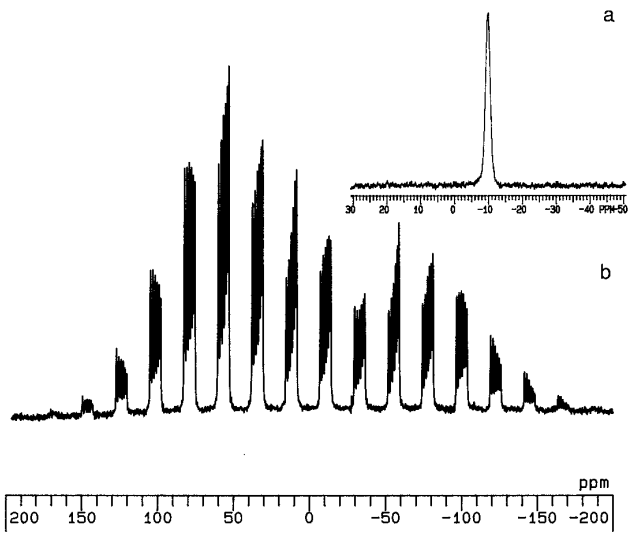

FIG. 1. (a) Solution and (b) solid-state ^{119}Sn NMR spectra of (*para*-$CH_3OC_6H_4)_3Sn(CO)_5Mn$ obtained at 111.725 MHz with proton decoupling. Solid-state experimental conditions: contact time 3 ms, recycle delay 3 s, number of transients 20,000.

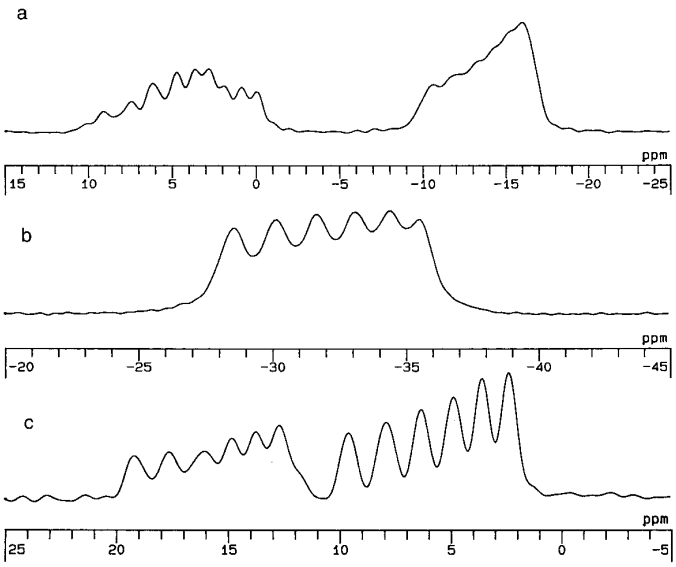

FIG. 2. Centerband regions of the ^{119}Sn NMR spectra of (a) $Ph_3Sn(CO)_5Mn$, (b) (*para*-$ClC_6H_4)_3Sn(CO)_5Mn$, and (c) (*para*-$FC_6H_4)_3Sn(CO)_5Mn$ showing distinct tin environments in the solid state. Experimental conditions: (a) contact time 1 ms, pulse delay 10 s, number of transients 5960; (b) contact time 3 ms, pulse delay 5 s, number of transients 12,000; (c) contact time 3 ms, pulse delay 4 s, number of transients 19,500. Spectra were obtained at 111.725 MHz with proton decoupling.

RESULTS AND DISCUSSION

When a spin-1/2 nucleus is bonded to a quadrupolar nucleus, the solid-state NMR spectrum is more complex than the solution spectrum (Fig. 1). The latter often shows only a single line without spin–spin coupling, whereas in the solid-state CP-MAS spectrum, multiplets with uneven spacings are observed. Examples of spin pairs involving either a $^{117/119}$Sn or ^{55}Mn nucleus for which such effects have been reported are (^{119}Sn, $^{35/37}$Cl) (*2, 3*), (^{13}C, ^{55}Mn) (*19*), and (^{31}P, ^{55}Mn) (*19–21*). The solid-state ^{119}Sn NMR spectrum of the $Ph_3Sn(CO)_5Mn$ system is complicated by the presence of four molecules in the asymmetric unit cell (*9*) with three resolvable isotropic chemical shifts (Fig. 2), whereas the spectra of the other complexes studied are much simpler, with one or two sets of isotropic chemical shifts and without any overlapping peaks in the solid-state spectra. The solid-state ^{119}Sn NMR spectrum of (p-$FC_6H_4)_3Sn$–$(CO)_5Mn$ consists of two sets of centerband multiplets, while the other complexes in the series, with the exception of $Ph_3SnMn(CO)_5$, exhibit a single set of centerband multiplets. This difference indicates that there are at least two distinct tin environments in solid (p-$FC_6H_4)_3Sn(CO)_5Mn$. X-ray data for (*para*-$FC_6H_4)_3Sn(CO)_5Mn$ show that it crystallizes in the space group $P\bar{1}$, with four molecules in the unit cell (*13*). Thus, the asymmetric unit contains two different molecules and two nonequivalent tin atoms, in excellent

agreement with the solid-state NMR data. The crystal structures of the remaining complexes were also determined, and were each found to contain one molecule in the asymmetric unit (*13*). These results are also consistent with those obtained from the solid-state ^{119}Sn NMR spectra.

The solid-state splittings have been explained by a first-order perturbation treatment for the high-field case (when the ratio of the quadrupolar to Zeeman frequency for the quadrupolar nucleus is small, $\chi/\nu_S < 1$), leading to the expression (*21*)

$$\Delta\nu_m = -mJ + (3\chi D''/10\nu_S) \times \{S(S+1) - 3m^2\}/\{S(2S-1)\}, \quad [3]$$

where $\Delta\nu_m$ is the shift produced by the m eigenstates of the quadrupolar nucleus (relative to the unperturbed isotropic shift frequency, ν_I), J is the isotropic I–S spin–spin coupling constant, ν_S is the resonance frequency of the quadrupolar nucleus, χ is the quadrupolar coupling constant (e^2qQ/h), and D'' is the effective dipolar coupling constant, including the anisotropy in the spin–spin coupling (ΔJ),

$$D'' = 1/2(D - \Delta J/3) \times (3\cos^2\beta^D - 1 + \eta\sin^2\beta^D\cos 2\alpha^D), \quad [4]$$

where η is the asymmetry in the electric field gradient **q**. The angular terms α^D and β^D describe the orientation of the internuclear vector $\mathbf{r}_{I-S}$, in the principal-axis system of the electric field gradient tensor **q**, with the assumption that the principal component of the J tensor is colinear with the internuclear vector and the tensor is assumed to be axially symmetric. The term D is the ^{119}Sn, ^{55}Mn direct dipolar coupling constant, given by

$$D = (\mu_0/4\pi)\gamma_{Sn(119)}\gamma_{Mn}h/(4\pi^2(\mathbf{r}_{Mn-Sn})^3). \quad [5]$$

From single-crystal, broad-line, ^{55}Mn NMR studies and molecular symmetry arguments (*22*), it was shown that the electric field gradient tensors are close to axial symmetry for $X_3Sn(CO)_5Mn(I)$ (X = Cl, Ph). X-ray structural analysis for these complexes (*9, 13*) revealed that the environment around the $Mn(CO)_5$ and Ar_3Sn moieties is indeed symmetric with close to C_{4v} and C_{3v} symmetry, respectively. This implies that the principal component of the electric field gradient, q_{zz}, lies near the internuclear vector $\mathbf{r}_{Mn-Sn}$ and the angular factors in Eq. [4] are small. In such circumstances, which are assumed for the triaryltin(pentacarbonyl)manganese(I) cases, there is a much simpler expression for D'':

$$D'' = (D - \Delta J/3). \quad [6]$$

Analysis of the splitting patterns (Fig. 3) was possible for all the complexes studied, by using Eq. [3], which resulted in the determination of the isotropic chemical shifts, δ_{iso}, the spin–spin coupling constants, $^1J_{Mn-Sn}$, and the effective dipolar–quadrupolar constants, $3\chi(D - \Delta J/3)/10\nu_S$ (Table 1). The isotropic shifts of the complexes in the solid state vary from those obtained from the solution-state NMR spectra, differing by as much as 33 ppm for the *para*-chloro

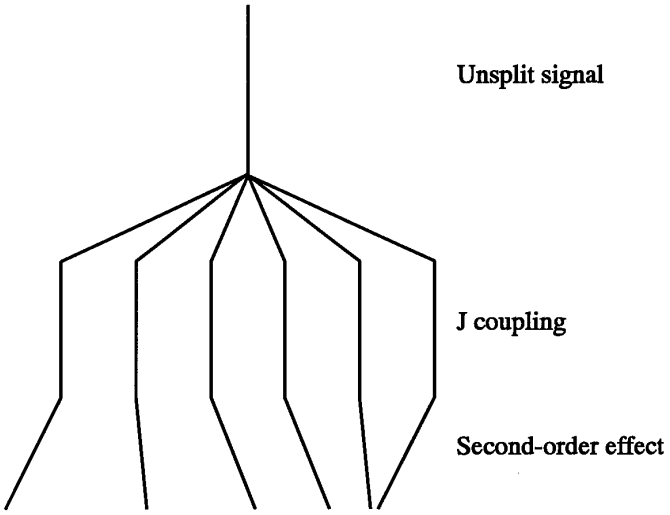

FIG. 3. Schematic representation of the spectrum of ^{119}Sn coupled to a single ^{55}Mn nucleus. Spin–spin coupling results in five equally spaced lines. First-order perturbation on the ^{119}Sn spectra arising from coupling to a quadrupolar nucleus, ^{55}Mn ($S = 5/2$), as a function of the parameter $\chi D''/\nu_S$.

TABLE 1
Solid-State and Solution ^{119}Sn NMR Isotropic Chemical Shifts and Coupling Constants of (*para*-XC$_6$H$_4$)SnMn(CO)$_5$[a]

X	δ_{iso} (soln)[b]	δ_{iso} (solid)[b]	J_{Mn-Sn} (solid) (Hz)	d[c] (HZ)
CH_3	−10.37	−16.6	132 (2)	33.3 (1.0)
H (a,b)[d]	−11.93	−13.6	135 (2)	34.4 (0.4)
H (c)	−11.93	2.82	141 (3)	30.3 (2.8)
H (d)	−11.93	5.66	141 (2)	34.3 (0.3)
OCH_3	−6.33	11.4	149 (1)	28.9 (0.8)
F (a)	−0.19	6.6	165 (2)	22.7 (0.5)
F (b)	−0.19	16.0	151 (2)	26.2 (0.8)
Cl	1.13	−32.1	160 (2)	25.7 (1.5)
SCH_3	−4.84	12.6	170 (1)	25.1 (0.2)
$S(O)_2CH_3$[e]	6.63	−10.1	250 (3)	36.1 (1.0)

[a] Values of isotropic shifts are in ppm, relative to external $(CH_3)_4Sn$.
[b] Uncertainties are ±0.05 and ±0.2 ppm for the solution and solid-state ^{119}Sn NMR spectra, respectively.
[c] $d = 3\chi D''/10\nu_s$.
[d] Two equivalent tin atoms.
[e] Spectrum was recorded on a Chemagnetics M-100 spectrometer operating at a field strength of 2.35 T.

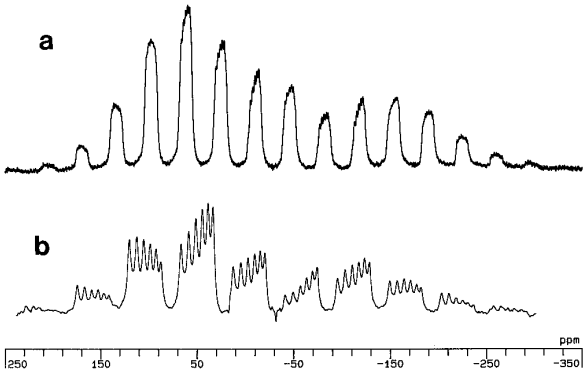

FIG. 4. Solid-state ^{119}Sn NMR spectra of (*para*-$CH_3S(O)_2C_6H_4)_3Sn(CO)_5Mn$ obtained at (a) 111.725 MHz and (b) 37.252 MHz with proton decoupling. Experimental conditions: (a) contact time 2 ms, pulse delay 1 s, number of transients 20,000; (b) contact time 2 ms, pulse delay 1 s, number of transients 2500.

complex. This is mainly due to the sensitivity of ^{119}Sn chemical shifts to the electronic environment and not to changes in coordination number of the tin or manganese nucleus in solution. This type of effect has also been observed for Ph_4Sn, Ph_3SnCl, and other tin complexes (*1*). The spin–spin coupling between ^{117}Sn or ^{119}Sn and ^{55}Mn, $^1J_{Mn-Sn}$, was not observed in the solution ^{117}Sn or ^{119}Sn NMR spectra due to fast quadrupolar relaxation processes. However, this coupling is observed in the solid-state ^{117}Sn and ^{119}Sn NMR spectra. The $^1J_{Mn-Sn}$ couplings were determined for most of the complexes at the two different fields, 7.05 and 2.35 T, and found to lie in the range of 132 to 250 Hz for the triaryltin complexes. It was difficult to resolve the peak positions of the centerband and sidebands of the spectrum obtained at 111.7 MHz for the sulfone derivative (Fig. 4). However, the centerband and the spinning sidebands of the spectrum, obtained for this compound at 37.2 MHz, are well resolved and the values of the spin–spin and effective dipolar–quadrupolar constants were easily determined. Both ^{117}Sn and ^{119}Sn NMR spectra were recorded for the *para*-SCH_3 complex, but only ^{119}Sn spectra were recorded for the other complexes, because of the lower receptivity of the ^{117}Sn nucleus. However, the reduced coupling constants (Eq. [7]) for the *para*-SCH_3 complex, $^1K(^{117}Sn, ^{55}Mn)$ and $^1K(^{119}Sn, ^{55}Mn)$, are found to be the same, -1.51×10^{21} T^2 J^{-1}, from both solid-state spectra:

$$^nK(Sn, Mn) = 4\pi^2\, {}^nJ(Sn, Mn)/(\gamma_{Sn}\gamma_{Mn})h. \qquad [7]$$

The δ_{iso} and $^1J_{Mn-Sn}$ values in the solid state are very sensitive to the electronic environment and to the nature of the *para*-substituents of the phenyl rings. For the two crystallographically nonequivalent molecules in $(p\text{-}FC_6H_4)_3Sn(CO)_5Mn(I)$, a slight change in the torsion angles of the phenyl rings modifies the environment around the tin atom, and thus causes differences in δ_{iso} and $^1J_{Mn-Sn}$, Table 1. However, modifying the *para*-substituents was found to cause drastic changes in $^1J_{Mn-Sn}$ (by as much as 120 Hz) and in δ_{iso} (up to 44 ppm).

The effective dipolar coupling constants and the quadrupole coupling constants cannot be separately determined from the effective dipolar–quadrupolar couplings, unless one of these quantities is known. The quadrupole coupling constants can be obtained experimentally from either NQR measurements or single-crystal NMR studies, but are notoriously difficult to determine for manganese complexes. Recently, it was shown by Gobetto *et al.* (*21*) that the effective dipolar coupling constant can be obtained from an analysis of spinning sideband manifolds,

$$\Delta\delta_{mI} = \Delta\delta_I - [2(D - \Delta J/3)/\nu_I]m_S, \qquad [8]$$

where $\Delta\delta_I$ is the shielding anisotropy of the I nucleus, $\Delta\delta_{mI}$ is the shielding anisotropy of the I spin for the m eigenstate of the S nucleus, and ν_I is the resonance frequency of the I spin. The values of D'', Eq. [6], were obtained from a regression plot of m vs $\Delta\delta_{mI}$, where the slope of the graph is equal to $-2(D - \Delta J/3)/\nu_I$ and the intercept equals $\Delta\delta_I$. The average values of D'' were determined from two or more spinning speeds and were found to lie in the range from -363 to -493 Hz. The values of χ, using Eq. [3], were then determined to be in the range -7.5 to 20 MHz (Table 2). The quadrupole coupling constant for the sulfone complex was negative, which implies that the principal axis of the electric field gradient has reversed direction. This may be due to the strong electron withdrawing ability of the

TABLE 2
Dipolar, Effective Dipolar, and Quadrupolar Coupling Constants, and Spin–Spin Anisotropy for (*para*-XC_6H_4)$SnMn(CO)_5$

X	D^a (Hz)	D'' [b] (Hz)	ΔJ [c] (Hz)	χ (MHz)
CH_3	−570.6 (2)	−363 (14)	622 (42)	20.4 (0.8)
H (a,b)	−582.9 (9)	−465 (6)	354 (4)	18.3 (0.1)[d]
H (c)	−582.3 (9)	−410 (38)	515 (33)	18.3 (0.1)[d]
H (d)	−582.3 (9)	−465 (4)	352 (4)	18.3 (0.1)[d]
OCH_3	−587.5 (2)	−455 (15)	398 (13)	16.4 (0.3)
F (a)	−594.8 (2)	−461 (14)	401 (13)	12.2 (0.4)
F (b)	−589.5 (2)	−401 (11)	566 (16)	16.2 (0.4)
Cl	−577.7 (2)	−476 (18)	305 (12)	13.4 (0.5)
SCH_3	−592.1 (2)	−425 (18)	501 (21)	14.6 (0.6)
$S(O)_2CH_3$	−591.5 (2)	−397 (10)	584 (15)	−7.52 (0.19)

[a] $D = (\mu_0/4\pi)(\gamma_{Mn}\gamma_{Sn}h/4\pi\mathbf{r}^3_{Mn-Sn})$; bond lengths from Ref. (*13*).
[b] From spinning sideband analysis; uncertainties were determined from three to four different spectra at different spinning speeds.
[c] $\Delta J = 3(D - D'')$.
[d] Values taken from Ref. (*22*).

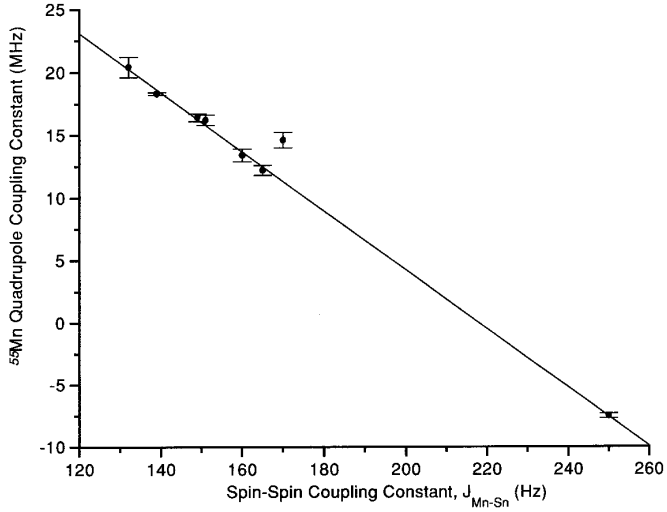

FIG. 5. Plot of the nuclear quadrupole coupling constant, χ (MHz) vs $^1J_{Mn-Sn}$, the $^{119}Sn-^{55}Mn$ spin–spin coupling constant (Hz), for the series (*para*-X $C_6H_4)_3Sn(CO)_5Mn$.

sulfone group, which results in a decrease of electron density at the tin atom.

From crystal structure data and spinning sideband analyses, the dipolar coupling constants, Eq. [5], and the anisotropies in the spin–spin coupling, Eq. [6], were determined to be in the range of −570 to −595 Hz and 268 to 622 Hz, respectively. The anisotropies of J are large and are similar in magnitude to the dipolar coupling constant and, therefore, should not be neglected in the calculation of the quadrupole coupling constant. The existence, however, of large ΔJ values suggests that the Fermi contact term is not the sole mechanism contributing to spin–spin coupling.

The quadrupole coupling constants of the complexes studied, Tables 1 and 2, decrease linearly with the increase in the one-bond spin–spin coupling between tin-119 and manganese, with the exception of the tris(*p*-methylthiophenyl)-tin derivative (Fig. 5). The relationship between χ and $^1J_{Mn-Sn}$ is due to the dominance of the Fermi contact term for $^1J_{Sn-Mn}$, which increases as the *s*-bonding character increases (Eq. [1]), and the nuclear quadrupole coupling constant which, according to the Townes and Dailey theory, decreases as the *s*-bonding character increases (Eq. [2]). The complexes studied are known to be strong covalent bimetallics so that the contribution of the *para*-substituents toward ionic character is minimal. Also, it is expected that the π-donation of electrons from the manganese $3d$ orbitals toward the empty $5d$ orbitals of the tin atom should remain constant through the series, since the $Mn(CO)_5$ fragment remains unchanged. The *para*-substituents on the phenyl rings either increase or decrease the donor–acceptor ability of the tin, due to inductive and/or resonance effects, which are then transmitted onto the tin atom. This results in an increase or decrease in the *s*-character of the hybrid orbital used by the tin nucleus in bonding to the manganese atom. Therefore, the relationship obtained from $^1J_{Sn-Mn}$ and χ is mainly due to the change in the *s*-bonding character of the tin and manganese bond.

The $(p\text{-}CH_3SC_6H_4)_3Sn(CO)_5Mn$ compound is yellow, which may suggest a smaller value for the average excitation energy term, ΔE, which is usually assumed to be constant for a similar series of complexes. The decrease in excitation energy may cause the spin–spin coupling constant for the thiomethyl derivative not to follow the χ versus $^1J_{Mn-Sn}$ behavior. The crystal structure of the tris(*p*-methylthiophenyl)tin compound (*13*) shows that its molecular structure differs from the other members of the $(p\text{-}X\,C_6H_4)Sn(CO)_5Mn$ series. The dihedral angle of one of the phenyl rings of this compound is −22°, far from the general range of 40° to 80° for such angles. It appears that these torsional

TABLE 3
^{119}Sn Chemical Shift Tensors for (*para*-XC_6H_4)SnMn(CO)$_5$[a,b]

X	δ_{11} (ppm)	δ_{22} (ppm)	δ_{33} (ppm)	$\Delta\delta$ (ppm)	η
CH_3	37.7	10.6	−97.3	−121.4	0.335
H (a,b)	71.6	2.8	−115.2	−152.4	0.677
H (c)	81.1	50.1	−122.8	−188.4	0.247
H (d)	89.4	47.3	−119.9	−188.3	0.335
OCH_3	125.1	54.3	−145.3	−235.0	0.452
F	77.2	77.2	−134.6	−211.8	0.000
	120.4	46.9	−119.2	−202.8	0.544
Cl	98.6	−39.4	−155.0	−184.6	0.885
SCH_3	171.7	82.3	−219.2	−346.2	0.417
$S(O)_2CH_3$[c]	167.5	58.1	−256.0	−368.8	0.445

[a] Uncertainties are ±1.5 and ±2.5 ppm for chemical shifts tensors and $\Delta\delta$, respectively.
[b] Anisotropy parameter $\Delta\delta = \delta_{33} - 1/2(\delta_{11} + \delta_{22})$ and $\eta = |\delta_{11} - \delta_{22}|/|\delta_{33} - \delta_{iso}|$, where $|\delta_{33} - \delta_{iso}| > |\delta_{11} - \delta_{iso}| > |\delta_{22} - \delta_{iso}|$.
[c] Spectrum was recorded on a Chemagnetics M-100 spectrometer operating at a field strength of 2.35 T.

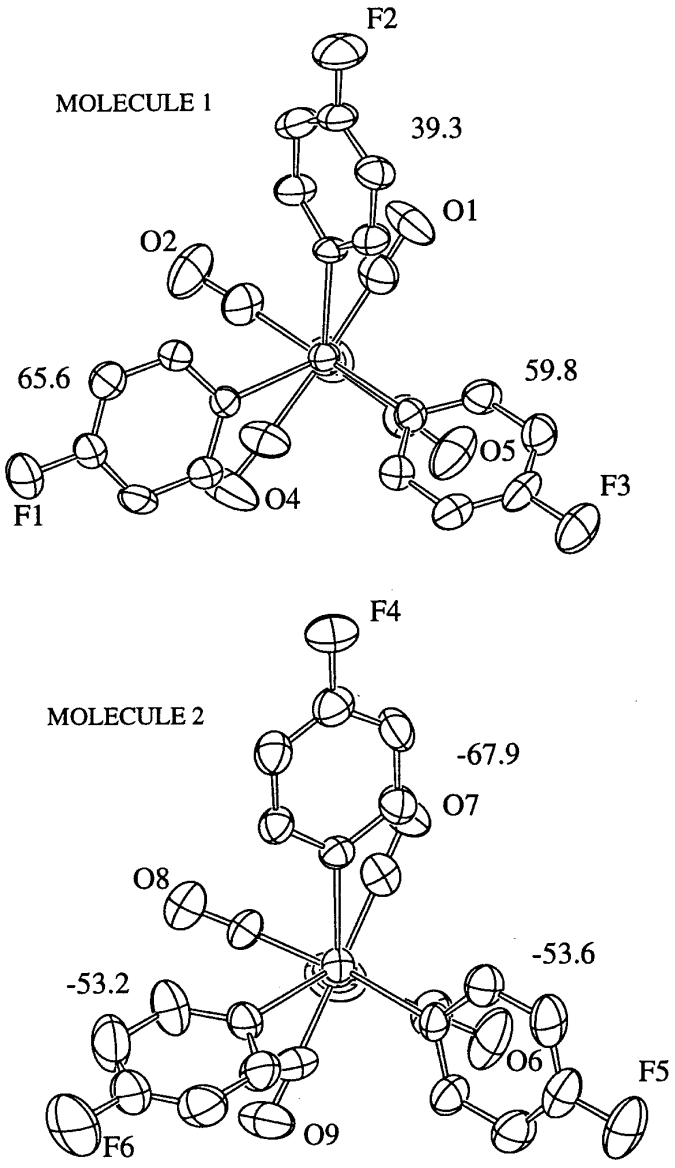

FIG. 6. Views of the two $(p\text{-}FC_6H_4)_3Sn(CO)_5Mn$ molecules perpendicular to the Mn–Sn axis showing the torsion angles of phenyl rings.

angles also have a profound influence on the components of the chemical shift tensor. For example, the phenyl ring torsion angles of $(p\text{-}CH_3C_6H_4)_3Sn-(CO)_5Mn$(I) are 56°, 69°, and 55° (*14*), and the chemical shift tensor values are 38, 11, and −97 ppm. In comparison, the *para*-SCH_3 derivative has torsion angles of 63°, 49°, and −22° (*13*), and tensor values of 172, 82, and −219 ppm. The large difference in torsion angle may influence the overlap of the π_{2pz} orbitals on the aromatic ring with the tin atom which can result in rehybridization for the $2p$ orbitals of the phenyl ring. This change in hybridization results in larger values for the tensor components, δ_{11} and δ_{22}.

The magnitudes and principal components of the tin chemical shifts tensors are given in Table 3. As $^1J_{Mn-Sn}$ increases, the tensor component δ_{33} increases, with the exception of the *para*-fluoro case. This result indicates that, as the *s*-bonding character increases, the δ_{33} value will increase if and only if the direction of δ_{33} is close to or along the tin–manganese bond. It was found from solid-state ^{119}Sn NMR measurements that there are two nonequivalent tin sites in the $(p\text{-}FC_6H_4)_3Sn(CO)_5Mn$ complex, which results in two sets of tensor quantities. One set of tensor values was determined, from spinning sideband analysis, to be symmetric while the other was asymmetric with an asymmetry factor, η, of 0.544. Crystal structure information (*13*) showed that there are two distinct molecules in the asymmetric unit, with torsion angles of −53°, −53°, −67° and 59°, 65°, 39° about the $Sn-C_{ipso}$ axis, Fig. 6. These results indicate that the orientation of δ_{33} at the tin atom should be such that it lies along the Mn–Sn bond for the X-ray and NMR data to agree. As a consequence, the remaining two components, δ_{11} and δ_{22}, must lie perpendicular to the δ_{33} axis. The tensor quantities δ_{11} and δ_{33} for the *para*-SCH_3 and *para*-$S(O)_2CH_3$ complexes are much larger in absolute value than those for the other members of the series. The OCH_3 and $S(O)_2CH_3$ substituents are the strongest electron donating and strongest electron withdrawing substituents, respectively, but there is no correlation between any of the shift tensor components with either Hammett or Taft constants. This observation is not surprising, since Hammett and Taft correlation constants are obtained from solution studies. The asymmetry factor ranges from 0 to 0.885 through the series, showing that δ_{11} and δ_{22} are very sensitive to the torsion angles of the phenyl ring and to the *para*-substituent on the phenyl ring.

ACKNOWLEDGMENTS

This research was supported by operating and equipment grants to D.F.R.G. and I.S.B. from the NSERC (Canada) and the FCAR (Quebec). We thank Drs. Kentgens, Power, and Wasylishen for the computer program for spinning sideband analysis.

REFERENCES

1. R. A. Komoroski, R. G. Parker, A. M. Mazany, and T. A. Early, *J. Magn. Reson.* **73,** 389 (1987).
2. R. K. Harris, *J. Magn. Reson.* **78,** 389 (1988).
3. (*a*) D. A. Apperley, B. Haiping, and R. K. Harris, *Mol. Phys.* **68,** 1277 (1989); (*b*) D. C. Apperley, N. A. Davies, R. K. Harris, A. K. Brimah, S. Eeller, and R. Fischer, *Organometallics* **9,** 2672 (1990).
4. H. Bai, R. K. Harris, and H. Reuter, *J. Organomet. Chem.* **408,** 167 (1991).
5. R. K. Harris, S. E. Lawrence, S. Oh, and V. G. Kumar Das, *J. Mol. Struct.* **347,** 309 (1995).
6. R. D. Gorsich, *J. Am. Chem. Soc.* **84,** 2486 (1962).
7. W. Jetz, P. B. Simons, J. A. J. Thompson, and W. A. G. Graham, *Inorg. Chem.* **5,** 2217 (1966).
8. A. Terzis, T. C. Strekas, and T. G. Spiro, *Inorg. Chem.* **13,** 1346 (1974).

9. H. P. Weber and F. R. Bryan, *Acta Crystallogr.* **22,** 822 (1967).

10. R. F. Bryan, *J. Chem. Soc. A,* 696 (1968).

11. R. F. Bryan, *J. Chem. Soc. A,* 172 (1967).

12. I. Wharf, *Inorg. Chim. Acta* **159,** 41 (1989).

13. (*a*) D. Christendat, I. Wharf, A. M. Lebuis, I. S. Butler, and D. F. R. Gilson, unpublished results; (*b*) D. Christendat, I. Wharf, A. M. Lebuis, I. S. Butler, and D. F. R. Gilson, 78th CSC Conference and Exhibition, Guelph, Ontario, May 28–June 1, 1995, paper 852.

14. C. Juan and H. S. Gutowsky, *J. Chem. Phys.* **37,** 2198 (1962).

15. B. P. Dailey and C. H. Townes, *J. Chem. Phys.* **23,** 118 (1955).

16. D. F. R. Gilson, *J. Chem. Phys.* **43,** 312 (1965).

17. R. K. Harris and A. Sebald, *Magn. Reson. Chem.* **25,** 1058 (1987).

18. A. P. M. Kentgens, W. Power, and R. E. Wasylishen, ''HBLQFIT Sideband Analysis,'' Version 2.2, Dalhousie University, Halifax, Nova Scotia, Canada.

19. D. Christendat, R. D. Markwell, D. F. Gilson, I. S. Butler, and J. D. Cotton, *Inorg. Chem.* **36,** 230 (1997).

20. E. Lindner, R. Fawzi, H. A. Mayer, K. Eichele, and K. Pohmer, *Inorg. Chem.* **30,** 1102 (1991).

21. R. Gobetto, R. K. Harris, and D. C. Apperley, *J. Magn. Reson.* **96,** 119 (1992).

22. J. L. Slater, M. Pupp, and R. K. Sheline, *J. Chem. Phys.* **57,** 2105 (1972).